Behavior of Belite cement blended with Calcium sulfoaluminate cement: an Ecocement

Angeles G. De la Torre [1,a], Diana Londono-Zuluaga[1,2,b], Juan Manuel Pineda[1,c]

[1]*Department of Inorganic Chemistry, Crystallography and Mineralogy, University of Malaga, Malaga, Spain*

[2]*Cement and Building Materials Group, National University of Colombia, Medellin, Colombia*

[a]mgd@uma.es
[b]dlondonoz@uma.es
[c]juanmapineda93@gmail.com

ABSTRACT

Belite Portland Cements (BPC) and calcium sulfoaluminate cements (CSA) are considered as environmentally friendly cements due to their lower CO2 emissions. These ecocements (BPC and CSA) emit about 0.03 and 0.18less tons of carbon dioxide from raw materials, respectively, than Ordinary Portland Cement (OPC).. However, BPCs have a technological disadvantage, due to the slow kinetic of hydration of belite (their main phase), causing low mechanical strengths at early ages. On the other hand, CSA cements are more expensive due their high alumina content, but they develop high mechanical strengths since early ages. Those are the main reasons why it is essential to develop strategies that could reduce their cost with competitive mechanical strengths.

A CSA clinker (ye'elimite as main phase) and a BPC (belite as main phase), have been mixed with the objective of producing a cheaper ecocement, labelled B#, that releases less CO2 than OPC and with competitive mechanical strengths. Cements with 83 wt%, 75 wt% and 65 wt% of BPC with CSA have been prepared. Moreover, anhydrite has been added as set regulator. Pastes with water/cement ratio of 0.4 have been prepared. The hydration of these pastes have been characterized by laboratory X-ray powder diffraction, using Rietveld methodology and thermogravimetric analysis, to obtain mineralogical phase assemblage as a function of time during a year, including amorphous content and free water. Mineralogical phase assemblage has been correlated to compressive strengths, porosity and dimensional stability of mortars.

1. INTRODUCTION

Great efforts have been directed to reduce energy consumption in Portland cement (PC) industry, in the last decades. PC production is a high energy demanding process, mainly due to fuel and electricity consumption. It is well stablished that cement industry contributes around 6% of all CO_2 anthropogenic emissions and consequently approximately 4% of the global warming of the planet (Barcelo et al., 2014).

Reducing these emissions can be achieved by several approaches (Monteiro et al., 2017) and the production of low calcite demanding cements is one of them. On the one hand, the production of Belite Portland Cements (BPC), where belite (C_2S) is the main phase, releases ~12-15% less CO_2 into atmosphere, due to less need of calcite and lower clinkering temperature. However, their slow reactivity leads to low mechanical strengths at early ages (Morsli et al., 2007). On the other hand, Calcium Sulfoaluminate cements (CSA), in which ye'elimite ($C_4A_3\bar{S}$) is the main phase, are binders most commonly used in China. They develop high mechanical strengths at early-ages and their production releases up to 40% less emissions than that of PC (Aranda & De la Torre, 2013). The main drawbacks of CSA cements are the variety of compositions, which causes a lack on normative for structural applications, and the high cost of raw materials.

Portland cement (PC) blended with additions based on calcium sulfoaluminate (CSA) are used in increasing amounts as special application mortars or concretes (Le Saoût et al., 2013). CSA are mainly added to provoke rapid setting cement with high early strengths or as a shrinkage compensator (Chaunsali & Mondal, 2016; Khalil et al., 2017; Sakai et al., 2004).

The main aim of this study is to obtain a low-CO_2 binder with competitive early and later mechanical strengths by blending BPC and CSA.

2. EXPERIMENTAL SECTION

2.1 Cement preparation.

A BPC clinker, supplied by Buzzi-Unicem (Italy), and a CSA clinker, manufactured in China and marketed in Europe by BELITH S.P.R.L. (Belgium) were mixed to prepared the blended cements. Moreover, anhydrite, prepared by heating (700°C for 60 min) commercial autoclaved alpha bassanite from BELITH S.P.R.L. (Belgium), was added as setting regulator. Table 1 gives the elemental composition determined by XRF for both BPC and CSA clinkers.

Table 1. Elemental compositions, expressed in weigh percentage of oxides excluding water and CO_2, of BPC and CSA clinkers.

Oxide	CaO	SiO_2	Al_2O_3	Fe_2O_3	SO_3	K_2O	Na_2O	MgO	TiO_2
BPC / wt%	59.7	22.9	5.2	2.1	5.4	1.1	0.3	2.9	-
CSA* / wt%	42.0	8.2	33.8	2.4	8.8	0.25	<0.08	2.7	1.5

* Also contains 0.15 wt% of SrO, 0.13 wt% of P_2O_5, 0.07 wt% of ZrO_2, 0.02 wt% of Cr_2O_3 and 0.01 wt% of MnO.

Three mixtures were prepared with BPC/CSA mass ratio of 83/17, 75/25 and 65/35, hereafter named as B83, B75 and B65, respectively. Table 2 gives the weight percentage of each component to prepared the cements. The calculated total CO_2 emissions due to clinkering of both components (considering calcite as calcium source) are 0.47, 0.45 and 0.42 T/T clinker produced for B83, B75 and B65 respectively.

Table 2. Weight percentages of each component of the cements.

Cement	BPC/ wt%	CSA/ wt%	Anhydrite/ wt%
B83	77.2	15.8	7
B75	68.3	22.7	9
B65	57.9	31.3	11

2.2 Paste preparation.

Cement pastes were prepared with deionized water using a water-to-cement (w/c) mass ratio of 0.4 following UNE-EN 196-3 standard. Superplasticizer (SP) (polycarboxylate-based, Floadis 1623, with 25 wt% of active matter, Adex Polymer S.L., Madrid, Spain) was added to the pastes to ensure homogeneity. The optimized amount of SP, active matter, was 0.4 wt% referred to cement for B83 and B75 and 0.5 wt% for B65. Pastes were poured into hermetically closed cylinders of polytetrafluoroethylene (PTFE), and were rotated during the first 24 h (16 rpm) at 20±1ºC. After that, all samples were kept under water at 20 ± 1ºC for 1, 7, 28 and 90 days. Prior to Laboratory X-Ray Powder Diffraction (LXRPD) and Differential ThermoAnalysis and ThermoGravimetric analysis (DTA-TG) characterization, the hydration of the cement pastes was arrested; for that, samples were firstly manually grinded, and then, the powder was washed and filtered twice with isopropanol, and once with diethyl ether.

2.3 Mortars preparation.

Mortars were prepared according to UNE-EN196-1 at cement/sand and w/c mass ratios of 1/3 and 0.4, respectively, and adding 0.4 and 0.5 wt% referred to blended cement of SP. CEN EN196-1 standard sand was used. Mortar cubes (3 × 3 × 3 cm^3) were cast and cured at 20±1°C and 99% relative humidity (RH) for 24 h. The cubes were demolded and kept in a water bath (20±1°C) until mechanical strength characterization (compression) was performed at 1, 7, 28 and 90 days.

2.4 Rheological characterization.

The amount of the superplasticiser was determined with a viscometer (Model VT550, Thermo Haake, Karlsruhe, Germany) with a serrated coaxial cylinder sensor, SV2P, provided with a lid to reduce evaporation. Flow curves were recorded using ramp times of 6 s in the shear rate range between 2 and 100 s^{-1}, for a total of 12 ramps. A further decrease from 100 to 2 s^{-1} shear rate was performed by following the same ramp times.

2.5 Mercury intrusion porosimetry (MIP)

MIP was carried out into cylindrical pieces (15 mm length and 10 mm diameter) of ~3 g mass which were first immersed in isopropanol for 72 h, and then dried at 40 ºC until their weight was stable. The surface of the cylinders was physically removed prior to the analysis. Micromeritics AutoPore IV 9500 porosimeter (Micromeritics Instrument Corporation, Norcross- GA, US) was used, which is capable of measuring porosity in the range from 1 mm down to 2 nm. The pressure applied by the intrusion porosimetry ranged from 0 to 300 MPa. A constant contact angle θ of 130° was assumed for data evaluation.

2.6 Mechanical strengths.

The compressive strengths of mortars were measured at 1, 7, 28 and 90 days and the reported value is the average of three measurements under the compression machine (Model Autotest 200/10 W, Ibertest, Madrid, Spain). The measured compressive strength values were corrected by the geometrical factor of 1.78 in order to obtain values comparable to those determined on using standard prisms (40x40x160 mm^3).

2.7 Laboratory X-ray Powder diffraction (LXRPD): data collection and analysis.

XRPD powder patterns were collected in flat transmission geometry (θ/θ), with the sample placed between two Kapton foils, in constant irradiated volume mode, on a D8 ADVANCE DaVinci (Bruker AXS, Germany) diffractometer. The diffractometer has a strictly monochromatic MoKα$_1$ radiation, λ=0.7093 Å obtained with a Johansson Ge (111) primary monochromator. The X-ray tube worked at 50 kV and 50 mA. The optics configuration was a 0.1º fixed divergence slit, and a 9 mm fixed diffracted anti-scatter slit. The energy-dispersive linear detector LYNXEYE XE 500 µm, optimized for high energy radiation, was used with the maximum opening angle. Using these conditions, the samples were measured between 3-35º (2θ) with a step size of 0.02º and with a total measurement time of 1 hour and 27 minutes by spinning the sample at 10 rpm.

All samples (anhydrous and hydrated) were mixed with ~20 wt% of SiO2 as internal standard to determine the Amorphous and non-Crystalline content, ACn (De la Torre et al., 2001).

2.8 Differential thermoanalysis and thermogravimetric analysis (DTA-TGA).

DTA-TGA were performed in a SDTQ600 analyzer (TA instrument, New Castle, DE) for every paste after the hydration was arrested. The measurements were carried out on ~30 mg of sample by heating up to 1000ºC at a heating rate of 10 ºC/min, in an open platinum crucible under air flow. The weight loss from RT to 600 ºC was computed to be chemically bounded water (used to calculate the free water, FW, content of the pastes as detailed in Zea-Garcia et al., 2019), and that from 600 to 1000ºC was considered as CO2. Derivative thermogravimetric (DTG) analysis will be plotted.

3. RESULTS

3.1 Rheological studies and mechanical strengths.

The amount of SP in every system was optimized through the rheological behavior of the corresponding pastes. Figure 1a shows selected flow curves for the three pastes prepared with different SP contents. In general, the viscosity of the pastes decrease by increasing the amounts of SP. Figure 1b shows the deflocculation curves of the three families at the shear rate of 50 s^{-1}, where the optimum value was achieved when 0.4 wt% SP was added to B83 and B75, while 0.5 wt% of SP was added to B65. Values were taken from the up-curves.

Figure 2 shows mechanical strengths up to 90 days of mortars prepared with the previous optimized SP content for each cement. BPC (data from internal communication) and CSA (García-Maté et al., 2015) mortars with w/c of 0.5 are included. As expected BPC mortars with higher w/c ratio developed lower mechanical strengths at all studied ages than blended mortars.

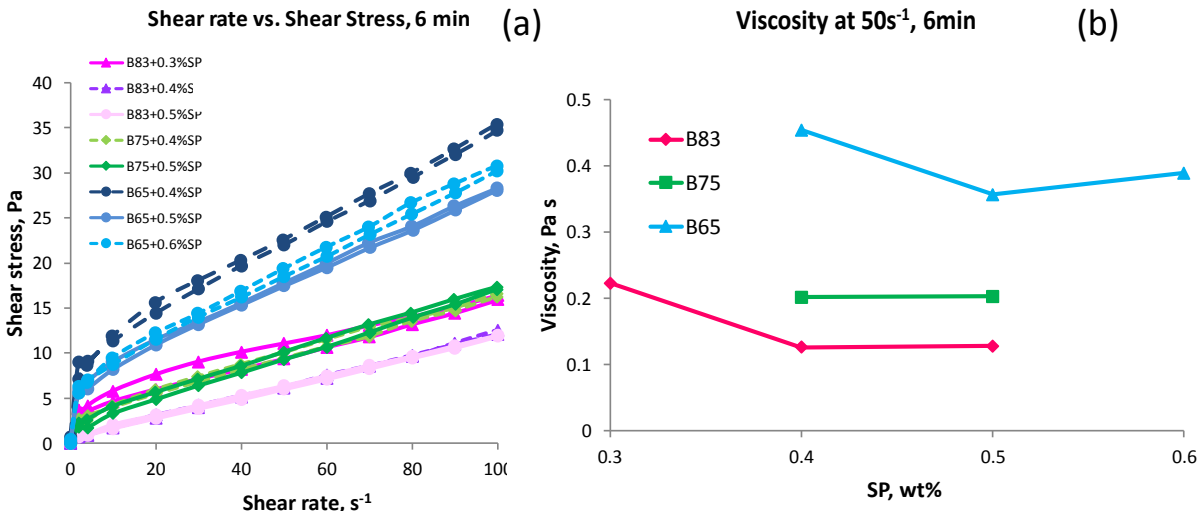

Figure 1. (a) Flow curves of B83, B75 and B65 pastes with different superplasticizer contents (water/cement ratio of 0.4). (b) Deflocculation curve of all the pastes prepared at a w/c ratio of 0.4 and different SP contents at the shear rate of 50 s^{-1} (values taken from the up-curves).

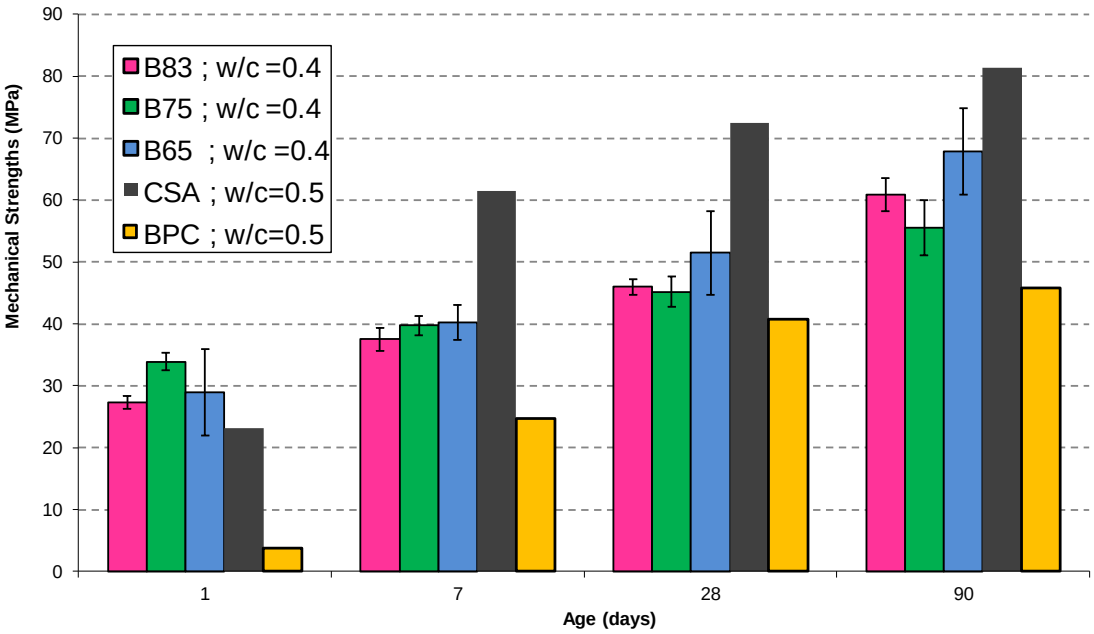

Figure 2. Compressive strengths for all the cements up to 90 days.

3.2 Laboratory X-ray powder diffraction results.

The hydration behaviour of all cement pastes, after stopping hydration as described in the experimental section, was studied at different curing ages. Figure 3 shows, as an example, raw LXRPD powder patterns as a function of time of hydration for B83 pastes, with main peaks due to a given phase labelled. Figure 4 gives the Rietveld plots of B65 anhydrous and at 90 days of hydration paste, as a representative example. Table 3 gives, as an example, the RQPA results of B83 pastes hydrated at 1, 7, 28 and 90, including ACn and FW contents. C_3S, C_3A, $C_4A_3\bar{S}$ and $C\bar{S}$ reacts from 1 day of hydration. However, C_2S is almost constant up to 28 days, Table 3. Main hydration products are ettringite or AFt [$C_6A\bar{S}_3H_{32}$] and stratlingite [C_2ASH_8], and in minor quantities of monosulfoaluminate or AFm [$C_4A\bar{S}H_{12}$] and Fe–Al siliceous hydrogarnet [$C_3(A,F)SH_4$].

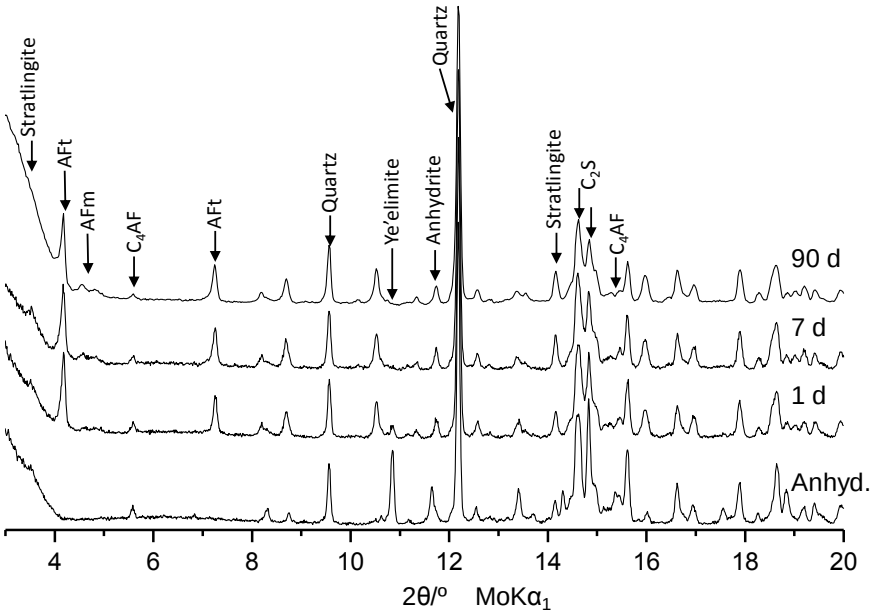

Figure 3. Raw LXRPD powder patterns of anhydrous B83 and the corresponding pastes for 1, 7 and 90 days of hydration, with main diffraction peaks due to a given phase labelled.

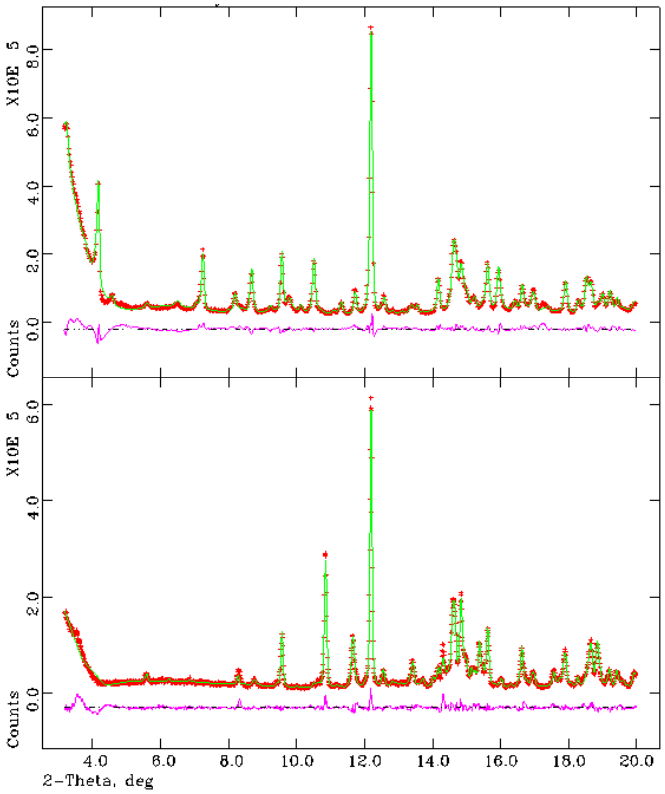

Figure 4. Rietveld LXRPD plots for anhydrous (bottom) and at 90 days of hydration paste (top) of B65, as a representative example, where red crosses are the experimental data, green line is the calculated pattern and purple line at the bottom is the different curve.

3.3 Porosimetry.

Figure 5 shows the average pore diameter determined by MIP for every paste as a function of hydration time.

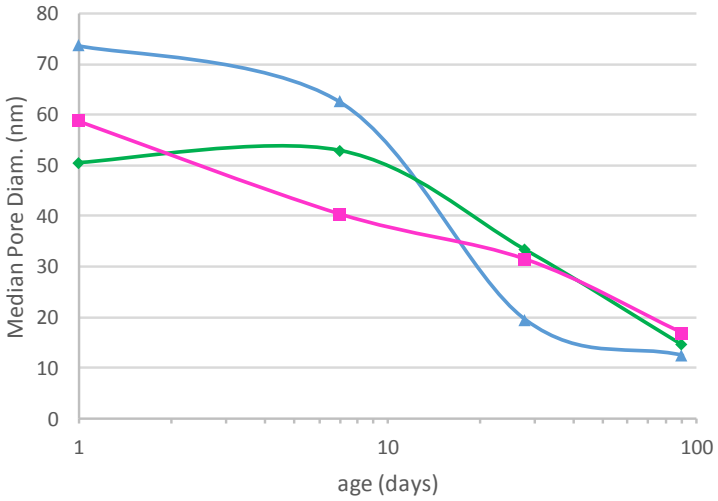

Figure 5. Average pore diameter determined by MIP for all the pastes.

Table 3. Full phase assemblage, determined by RQPA including ACn and FW, of B85 pastes.

Phases	t_0	1d	7d	28d	90d
C_3S	8.9	4.8	2.3	2.5	2.0
C_2S	29.0	32.9	34.0	34.5	25.5
C_3A	0.7	0.7	0.0		-
C_4AF	5.4	3.5	3.6	2.9	1.7
$C_4A_3\bar{S}$	7.1	1.4	-	-	-
MgO	1.6	1.5	1.5	1.4	1.2
$C\bar{S}$	4.9	-	-	-	-
AFt	-	20.4	20.3	20.3	18.5
Stratlingite	-	4.3	9.7	3.7	6.0
$C_3(A,F)SH_4$	-	-	-	-	1.0
AFm	-	-	-	-	0.8
ACn	13.8	19.1	20.2	25.7	37.6
FW	28.6	11.5	8.3	9.0	5.6

4. DISCUSSION

Reaction mechanism of plain CSA is very quick, i.e. first hours of hydration, and is dominated by the amount of ye'elimite and anhydrite by reaction (1), in which ettringite and amorphous AH_3 are formed.

$$C_4A_3\bar{S} + 2\,C\bar{S} + 38\,H \rightarrow C_6A\bar{S}_3H_{32} + 2\,AH_3 \quad (1)$$

Moreover, one of the main phases of BPC, C3S, reacts in the first hours of hydration to produce C-S-H gel and CH, reaction (2) (Cuesta et al., 2018).

$$C_3S + 5.3\,H \rightarrow C_{1.8}SH_4 + 1.2\,CH \quad (2)$$

When PC is blended with CSA the mechanism of hydration at first hours is according to reaction (3) (Chaunsali & Mondal, 2016):

$$C_4A_3\bar{S} + 8\,C\bar{S} + 6\,CH + 76\,H \rightarrow 3\,C_6A\bar{S}_3H_{32} \quad (3)$$

As observed in Table 3, AFt is formed in great quantities since 1 day of hydration, and after this time is almost constant in all the cements. The precipitation of large amounts of AFt at early ages is highly favourable and desirable as at this time the pastes show a higher plasticity which can better accommodate the precipitation of ettringite (García-Maté et al., 2015). Figure 6a shows the amount of AFt formed by each blended cement with hydration time. It can be observed that after one day the cement with higher amounts of AFt at all hydrating ages is B65, as expected, as it contains more CSA. Furthermore, it can also be observed that the amount of AFt slightly decreases at 90 days of hydration in B85 and B75 cements. This is due to due to the reactivity of C3S and C2S which create a rich siliceous environment and yield to the instability of AFt (Chitvoranund et al., 2016; Londono-Zuluaga et al., 2017; Rolland et al., 2014). Ettringite is, therefore, partly descomposed and AFm is formed.

On the other hand, stratlingite, C_2ASH_8 can be formed by the reaction of belite (and/or alite) with amorphous AH_3, reactions (4) and (5), respectively.

$$C_2S + AH_3 + 5H \rightarrow C_2(A,S)H_8 \quad (4)$$

$$C_3S + AH_3 + 6H \rightarrow C_2ASH_8 + CH \quad (5)$$

Stratlingite is also formed at low quantities since 1 day of hydration, Figure 6a, and in great quantities in B85, up to 7 days. However, after 90 days, B65 is the cement with higher amounts of stratlingite due to reaction (4). We can conclude that the presence of CSA has yielded higher quantities of aluminium hydroxide which has enhanced the formation of stratlingite. This has decreased the medium pore size diameter, Figure 5, and increase mechanical strengths, Figure 2.

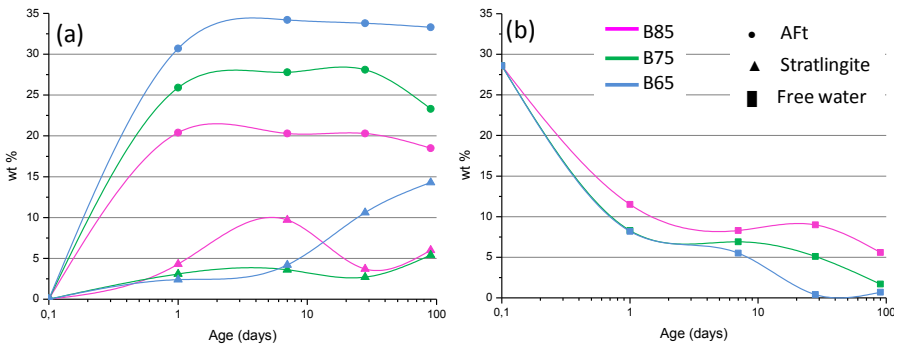

Figure 6. (a) Weight percentage of AFt (circles) and stratlingite (triangles) as a function of time for all the blended cements. (b) Free water at all hydration times for all the blended cements (squares).

The presence of stratlingite, which is a highly disordered phase and difficult to quantify by RQPA (Santacruz et al., 2016), was also proved by DTG-TG, see Figure 7. In this figure the two signals associated to the decomposition of stratlingite are larger for B65 than for the other binders. Moreover, Figure 7 also shows the absence of portlandite in these pastes, due to the lack of a signal at ~450ºC. This phase was mainly formed from reaction (4), although some authors stated that stratlingite is formed from the reaction between C-S-H gel and AH_3 as secondary reaction (Palou et al., 2005)

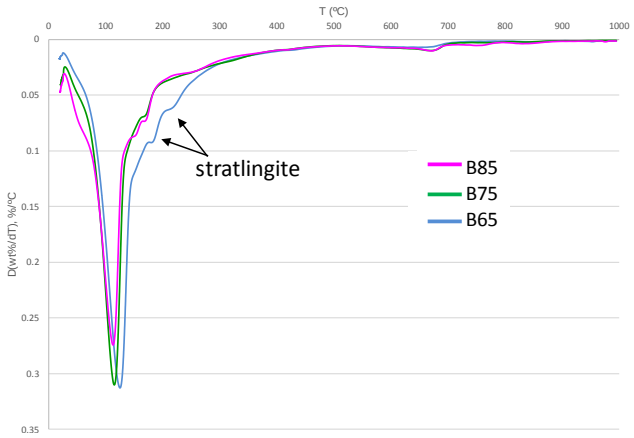

Figure 7. Derivative TG curves for 90 day pastes of the three blended cement studied.

B65 paste after 28 days of hydration is the one with less amount of free water (FW), Figure 6b. Moreover, the average pore diameter of B65 decreases at a higher pace from 28 days of hydration than the other pastes, Figure 5. Consequently, the higher amount of stratlingite and AFt (with the corresponding lower amount of FW) causes the diminution of pore diameter and justify the higher mechanical strengths developed by B65 mortars at 28 and 90 days of hydration, Figure 2.

5. CONCLUSIONS

This work indicates that BPC blended with higher amounts of CSA increase not only early age mechanical strengths of but also later age ones, i.e. 28 days. All mixtures have developed higher mechanical strengths than plain BPC (although this result has to be taken with caution since mortars with different w/c ratio have been compared). At 1 day of hydration, the mixture with 25 wt% of CSA, B75, has developed the highest mechanical strengths. B65 cement developed lower mechanical strengths at 1 day of hydration, in spite of having higher amounts of ettringite, due to the higher pore diameter size. However, B65 cement has developed the highest (of the three studied cements) mechanical strengths at 28 and 90 days, 51.5 MPa and 67.9 MPa, respectively. These mechanical strength increase is justified by higher amounts of stratlingite at these ages in B65. This phase is formed by the reaction of belite with water in the presence of aluminium hydroxide, the later coming from ettringite formation reaction. Moreover, ettringite is more stable in cements with poorer silicate rich environment, i.e. B65.

6. ACKNOWLEDGEMENTS.

Funding from Spanish MINECO BIA2017-82391-R, which is co-funded by FEDER is acknowledged. PhD. Londono-Zuluaga was funded by Beca Colciencias 646—Doctorado en el exterior and Enlaza Mundos 2013 program grant which is thanked. PhD Londono-Zuluaga is currently at Laboratory of Construction Materials (LMC), EPFL STI IMX LMC Station 12, 1015 Lausanne, (Switzerland). Authors thanks PhD. Fulvio Canonico and PhD. Daniela Gastaldi from BuzziUnicem for supplying the BPC material and for the discussion of the results.

7. REFERENCES

Aranda, M. A. G., & De la Torre, A. G. (2013). Sulfoaluminate cement in Eco-efficient concrete; Pacheco-Torgal, F. Ed.; Jalali, S. Ed. Labrincha, J. Ed. Woodhead Publishing: Cambridge, 488–522.

Barcelo, L., Kline, J., Walenta, G., & Gartner, E. (2014). Cement and carbon emissions. Materials and Structures, 47(6), 1055–1065.

Chaunsali, P., & Mondal, P. (2016). Physico-chemical interaction between mineral admixtures and OPC-calcium sulfoaluminate (CSA) cements and its influence on early-age expansion. Cement and Concrete Research, 80, 10–20.

Chitvoranund, N., Lothenbach, B., Winnefeld, F., & Hargis, C. W. (2016). Synthesis and hydration of alite-calcium sulfoaluminate cement. Advances in Cement Research, 29(3), 101–111.

Cuesta, A., Zea-Garcia, J. D., Londono-Zuluaga, D., De la Torre, A. G., Santacruz, I., Vallcorba, O., Aranda, M. A. G. (2018). Multiscale understanding of tricalcium silicate hydration reactions. Scientific Reports, 8(1), 8544.

De La Torre, A. G., Bruque, S., & Aranda, M. A. G. (2001). Rietveld quantitative amorphous content analysis. Journal of Applied Crystallography, 34(2), 196–202.

García-Maté, M., De La Torre, A. G., León-Reina, L., Losilla, E. R., Aranda, M. A. G. A. G., & Santacruz, I. (2015). Effect of calcium sulfate source on the hydration of calcium sulfoaluminate eco-cement. Cement and Concrete Composites, 55, 53–61.

Khalil, N., Aouad, G., El Cheikh, K., & Rémond, S. (2017). Use of calcium sulfoaluminate cements for setting control of 3D-printing mortars. Construction and Building Materials, 157, 382–391.

Le Saoût, G., Lothenbach, B., Hori, A., Higuchi, T., & Winnefeld, F. (2013). Hydration of Portland cement with additions of calcium sulfoaluminates. Cement and Concrete Research, 43, 81–94.

Londono-Zuluaga, D., Tobon, J. I., Aranda, M. A. G., Santacruz, I., & De La Torre, A. G. (2017). Clinkering and hydration of Belite-Alite-Ye´elimite cement. Cement and Concrete Composites, 80, 333–341.

Monteiro, P. J. M., Miller, S. A., & Horvath, A. (2017). Towards sustainable concrete. Nature Materials, 16(7), 698-699.

Morsli, K., De La Torre, Á. G., Stöber, S., Cuberos, A. J. M., Zahir, M., & Aranda, M. A. G. (2007). Quantitative phase analysis of laboratory-active belite clinkers by synchrotron powder diffraction. Journal of the American Ceramic Society, 90(10), 3205–3212.

Palou, M., Majling, J., Dová, M., Kozanková, J., Mojumdar, S. C. (2005) Formation and stability of crystallohydrates in the non-equilibrium system during hydration of SAB cements. Ceramics Silikáty, 49, 230-236

Rolland, L., Trauchessec, R., Institut, D. L., Lamour, J., & Rolland, B. Le. (2014). Impact of anhydrite proportion in a calcium sulfoaluminate cement and Portland cement blend. Advances in Cement Research, 26(6), 325–333.

Sakai, E., Nikaido, Y., Itoh, T., & Daimon, M. (2004). Ettringite formation and microstructure of rapid hardening cement. Cement and Concrete Research, 34(9), 1669–1673.

Santacruz, I., De la Torre, Á. G., Álvarez-Pinazo, G., Cabeza, A., Cuesta, A., Sanz, J., & Aranda, M. A. G. (2016). Structure of stratlingite and effect of hydration methodology on microstructure. Advances in Cement Research, 28(1), 13–22.

Zea-Garcia, J. D., Santacruz, I., Aranda, M. A. G., & De la Torre, A. G. (2019). Alite-belite-ye'elimite cements: Effect of dopants on the clinker phase composition and properties. Cement and Concrete Research, 115, 192–202.